



# Conceptual Models of Entrainment, Jet Lag, and Seasonality

Isao T. Tokuda<sup>1</sup>, Christoph Schmal<sup>2</sup>, Bharath Ananthasubramaniam<sup>3</sup> and Hanspeter Herzel<sup>2,3\*</sup>

<sup>1</sup> Department of Mechanical Engineering, Ritsumeikan University, Kyoto, Japan, <sup>2</sup> Institute for Theoretical Biology, Humboldt Universität zu Berlin, Berlin, Germany, <sup>3</sup> Institute for Theoretical Biology, Charité—Universitätsmedizin Berlin, Berlin, Germany

## OPEN ACCESS

### Edited by:

Rodolfo Costa,  
University of Padova, Italy

### Reviewed by:

Eva C. Winnebeck,  
Ludwig Maximilian University of  
Munich, Germany  
Elizabeth B. Klerman,  
Harvard Medical School,  
United States  
Luisa K. Pilz,  
Federal University of Rio Grande do  
Sul, Brazil

### \*Correspondence:

Hanspeter Herzel  
h.herzel@biologie.hu-berlin.de

### Specialty section:

This article was submitted to  
Chronobiology,  
a section of the journal  
Frontiers in Physiology

Received: 18 November 2019

Accepted: 23 March 2020

Published: 28 April 2020

### Citation:

Tokuda IT, Schmal C,  
Ananthasubramaniam B and Herzel H  
(2020) Conceptual Models of  
Entrainment, Jet Lag, and Seasonality.  
Front. Physiol. 11:334.  
doi: 10.3389/fphys.2020.00334

Understanding entrainment of circadian rhythms is a central goal of chronobiology. Many factors, such as period, amplitude, *Zeitgeber* strength, and daylength, govern entrainment ranges and phases of entrainment. We have tested whether simple amplitude-phase models can provide insight into the control of entrainment phases. Using global optimization, we derived conceptual models with just three free parameters (period, amplitude, and relaxation rate) that reproduce known phenotypic features of vertebrate clocks: phase response curves (PRCs) with relatively small phase shifts, fast re-entrainment after jet lag, and seasonal variability to track light onset or offset. Since optimization found multiple sets of model parameters, we could study this model ensemble to gain insight into the underlying design principles. We found complex associations between model parameters and entrainment features. *Arnold* onions of representative models visualize strong dependencies of entrainment on periods, relative *Zeitgeber* strength, and photoperiods. Our results support the use of oscillator theory as a framework for understanding the entrainment of circadian clocks.

**Keywords:** circadian rhythms, amplitude-phase model, parameter optimization, jet lag, phase response curve, entrainment, seasonality

## 1. INTRODUCTION

### 1.1. Entrainment and Oscillator Theory

The circadian clock can be regarded as a system of coupled oscillators. Examples include the neuronal network in the SCN (Hastings et al., 2018) and the “orchestra” of body clocks (Dibner et al., 2010). Furthermore, the intrinsic clock is entrained by *Zeitgebers*, such as light, temperature, and feeding. The concept of interacting oscillators (Van der Pol and Van der Mark, 1927; Kuramoto, 1984; Huygens, 1986; Strogatz, 2004) can contribute to the understanding of entrainment (Winfree, 1980). The theory of periodically driven self-sustained oscillators leads to the concept of “*Arnold* tongues” (Glass and Mackey, 1988; Pikovsky et al., 2003; Granada et al., 2009). *Arnold* tongues predict the ranges of periods and *Zeitgeber* strengths in which entrainment occurs (Abraham et al., 2010). The range of *Zeitgeber* periods over which entrainment occurs is called the “range of entrainment” (Aschoff and Pohl, 1978). If seasonal variations are also considered, the entrainment regions are termed “*Arnold* onions” (Schmal et al., 2015). Within these parameter regions, amplitudes and entrainment phases can vary drastically. Amplitude expansion due to external periodic driving is termed “resonance” (Duffing, 1918). Of central importance in chronobiology is the variability of the entrainment phase, since it allows the coordination of the intrinsic clock phase with the environment (Aschoff, 1960). Appropriate periods also provide evolutionary advantages (Ouyang et al., 1998; Dodd et al., 2005).

## 1.2. Phenomenological Amplitude-Phase Models

After the discovery of transcriptional feedback loops (Hardin et al., 1990), many mathematical models have focused on gene-regulatory networks (Forger and Peskin, 2003; Leloup and Goldbeter, 2003; Becker-Weimann et al., 2004). More recent models include many details of the transcriptional-translational feedback loops (Zhou et al., 2015; Bellman et al., 2018). However, most available data on phase response curves (PRCs) (Johnson, 1992), entrainment ranges (Aschoff and Pohl, 1978), and phases of entrainment (Rémi et al., 2010) are based on organismic data. Thus, it seems reasonable to study phenomenological models that are directly based on these empirical features. There is a long tradition of heuristic amplitude-phase models in chronobiology (Klotter, 1960; Wever, 1962; Pavlidis, 1973; Daan and Berde, 1978; Winfree, 1980; Kronauer et al., 1982).

Amplitude-phase models are quite generic and could be applied to any organism. We have adapted the entrainment features, discussed below in detail, to observed data of mammals (Daan and Aschoff, 1975; Reddy et al., 2002; Comas et al., 2006). Here, we have examined the capability of such heuristic amplitude-phase models to reproduce fundamental properties of circadian entrainment. To this end, we combine the traditional amplitude-phase modeling approach with recent oscillator theory and global optimization to identify minimal models that can reproduce essential features of mammalian clocks: PRCs with relatively small phase shifts (Honma et al., 2003), fast re-entrainment after jet lag (Yamazaki et al., 2000), and seasonal variability (Daan and Aschoff, 1975).

## 1.3. Entrainment Features and Model Constraints

Intrinsic periods of various organisms approximate in general the daylength of 24 h (Wyse et al., 2010). For example, *Neurospora* strains exhibit periods between 21 and 27 h (Lakin-Thomas et al., 1991; Merrow et al., 1999; Loros and Dunlap, 2001). Nocturnal rodents typically exhibit periods between 23 and 24 h in constant darkness (Pittendrigh and Daan, 1976a), whereas humans mostly exhibit periods slightly above 24 h (Wever, 1979; Czeisler et al., 1999). *Zeitgeber* signals, such as light, can accelerate or decelerate intrinsic rhythms leading to entrainment. PRCs quantify the amplitude and direction of phase shifts induced by *Zeitgeber* pulses (Wever, 1964; Johnson, 1992). In mammals, the strong coupling of SCN neurons constitutes a strong oscillator (Abraham et al., 2010; Granada et al., 2013), which has PRCs with relatively small phase shifts (Comas et al., 2006). Even bright light pulses of 6.7 h duration can shift the clock by just a few hours (Khalsa et al., 2003). These observations constitute the first constraint on our models. We assume that the maximal phase shifts are just 1 or 2 h.

Small phase shifts due to the *Zeitgeber* can lead to long transients of phase relaxation after jet lag (Kori et al., 2017). In many cases, a surprisingly fast recovery from jet lag is observed (Reddy et al., 2002; Vansteensel et al., 2003). These findings lead to our second model constraint. Along the lines of a previous optimization study (Locke et al., 2008), we request

that our models reduce the jet lag-induced phase shift by 50 % within 2 days.

The third constraint refers to the well-known seasonal variability of circadian clocks (Pittendrigh and Daan, 1976b; Hazlerigg and Wagner, 2006; Rémi et al., 2010). It has been reported that phase markers can lock to dusk or dawn for varying daylengths. This implies that the associated phases change by 4 h, if we switch from 16:8 LD conditions to 8:16 LD conditions. Thus, we also optimize our models to exhibit such pronounced phase differences between 16:8 and 8:16 LD cycles.

After having introduced our model and the optimization procedure in the Methods section, we have tested whether or not simple amplitude-phase models can reproduce the three entrainment features discussed above.

## 2. METHODS

### 2.1. Optimization of the Amplitude-Phase Model

As a model of an autonomous circadian clock, we consider the following amplitude-phase oscillator (Glass and Mackey, 1988; Abraham et al., 2010):

$$\frac{dr}{dt} = \lambda r(A - r), \quad (1)$$

$$\frac{d\varphi}{dt} = \omega = \frac{2\pi}{\tau}. \quad (2)$$

The system is described in polar coordinates by radius  $r$  and angle  $\varphi$  and has a limit cycle with amplitude  $A$  and angular frequency  $\omega$  (or period  $\tau$ ). Any perturbation away from the limit cycle will relax back with a relaxation rate  $\lambda$ . This oscillator model can be represented in cartesian  $(x, y)$  coordinates as

$$\frac{dx}{dt} = -\lambda x(r - A) - \omega y + Z(t), \quad (3)$$

$$\frac{dy}{dt} = -\lambda y(r - A) + \omega x, \quad (4)$$

where  $r = \sqrt{x^2 + y^2}$ . The oscillator receives a *Zeitgeber* signal

$$Z(t) = \begin{cases} 1 & \text{if } t \bmod T < \kappa T \\ 0 & \text{otherwise,} \end{cases} \quad (5)$$

where  $T$  represents the period of the *Zeitgeber* signal, and  $\kappa$  determines the photoperiod (i.e., fraction of time during  $T$  hours when the lights are on). Amplitude-phase models provide the simplest mathematical framework to study limit cycle oscillations, which have been discussed in the context of circadian rhythms (Wever, 1962; Winfree, 1980; Kronauer et al., 1982).

The amplitude-phase model (1), (2) has three unknown parameters  $\{A, \omega, \lambda\}$ . These parameters were optimized to satisfy the model constraints described in 1.3. The parameter optimization is based on the minimization of a cost function. The cost function takes a set of parameters as arguments, evaluates the model using those parameters, and then returns a “score” indicating the goodness of fit. Scores may only be positive, where

a fit with score closer to zero represents a better fit. The cost function is given by

$$E(A, \omega, \lambda) = \frac{(T_e - 48h)^2}{(24h)^2} + \frac{(\Delta\varphi_{max} - 1h)^2}{(1h)^2} + \frac{(\Delta\psi - 4h)^2}{(4h)^2}, \quad (6)$$

where  $T_e$ ,  $\Delta\varphi_{max}$ , and  $\Delta\psi$  represent half-time to re-entrainment, maximum phase-shift, and seasonal phase variability, respectively. The denominators can be regarded as tolerated ranges. If the values of  $T_e$ ,  $\Delta\varphi_{max}$ , and  $\Delta\psi$  deviate 24, 1, and 4 h from their target values, a score of three results. All parameter sets discussed in this paper had optimized scores below 0.1, i.e., the constraints are well-satisfied. Below we describe in detail how our quantities  $T_e$ ,  $\Delta\varphi_{max}$ , and  $\Delta\psi$  were calculated.

When the circadian oscillator is entrained to the *Zeitgeber* signal, their phase difference  $\psi = \Psi - \varphi$  ( $\Psi = 2\pi t/T$ : phase of the *Zeitgeber*) converges to a stable phase  $\psi_e$ , which is called the “phase of entrainment.” The half-time to re-entrainment  $T_e$  denotes the amount of time required for the oscillator to recover from jet lag. As the *Zeitgeber* phase is advanced by  $\Delta\Psi$ , the phase difference becomes  $\psi = \psi_e + \Delta\Psi$ .  $T_e$  quantifies how long it takes until the advanced phase is reduced to less than half of the original shift due to jet lag (i.e.,  $|\psi - \psi_e| < 0.5\Delta\Psi$ ). In our computation, this quantity was averaged over 24 different times during the day, at which 6h-advanced jet lag was applied. Next, the seasonal phase variability, which quantifies variability of the phase of entrainment over photoperiod from long day (16:8 LD) to short day (8:16 LD), is computed as  $\Delta\psi = \max_{x \in [1/3, 2/3]} \psi_e - \min_{x \in [1/3, 2/3]} \psi_e$ . Finally, the maximum phase-shift is given by  $\Delta\varphi_{max} = \max_{\varphi} |PRC(\varphi)|$ , where  $PRC(\varphi)$  represents PRC of the free-running oscillator, to which a 6 h light pulse is injected at its phase of  $\varphi$ .

To find optimal parameter values, the cost function was minimized by a particle swarm optimization algorithm (Eberhart and Kennedy, 1995; Trelea, 2003). Search ranges of the parameter values were set to  $A \in [0, 5]$ ,  $\omega \in [2\pi/30 \text{ rad/h}, 2\pi/18 \text{ rad/h}]$ ,

$\lambda \in [0h^{-1}, 0.5h^{-1}]$ . Altogether 600 sets of parameter values were obtained. From the estimated parameters, the intrinsic period was obtained as  $\tau = 2\pi/\omega$ .

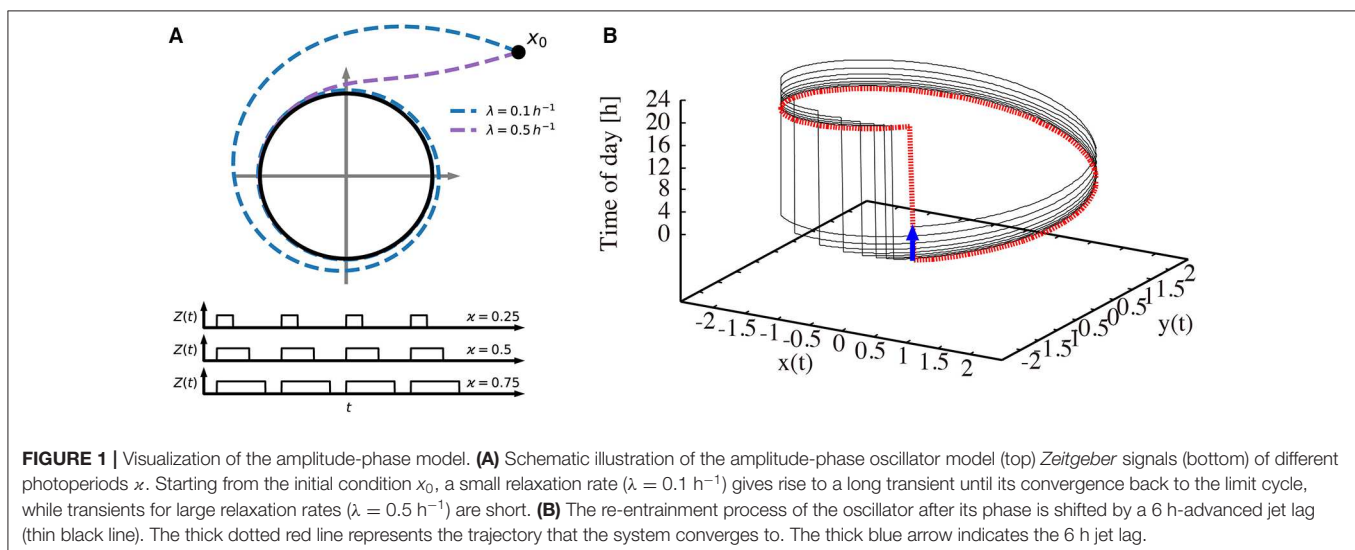
## 2.2. Simulations of Jet Lag, Phase Response, and Seasonality

**Figure 1** illustrates our modeling approach. In **Figure 1A**, the amplitude-phase equations (1) and (2) are visualized in the phase plane together with the driving *Zeitgeber* switching between 0 (dark) and 1 (light) for varying photoperiods. Two values of the amplitude relaxation rate  $\lambda$  illustrate how  $\lambda$  affects the decay of perturbations. Starting from an initial condition, a small relaxation rate gives rise to a long transient until its convergence to the limit cycle, while systems with large relaxation rates exhibit only a short transient. **Figure 1B** shows the oscillations in a 3-dimensional phase space. Two coordinates ( $x$  and  $y$ ) span the phase plane of the endogenous oscillator. The vertical axis represents the phase of the *Zeitgeber*. The dotted red line marks the periodically driven limit cycle. The jump from 24 to 0 h reflects simply the periodic nature of our daily time.

Interestingly, the relaxation after jet lag can be visualized as a transient convergence to the dotted red limit cycle via the black line after a 6 h phase change due to jet lag (blue arrow). Such a relaxation might be accompanied by amplitude changes (not apparent in the figure) and by steady phase shifts from day to day (note that the jump from 24 to 0 h is shifted day by day). After a few days, the dotted red line is approached, implying a vanishing jet lag. More conventional visualizations of the recovery from jet lag are given in **Figure 2**.

## 2.3. Global Sensitivity Analysis

To study the dependencies of the entrainment features on the model parameters, Sobol’s global sensitivity analysis was carried out (Sobol, 1993, 2001; Morio, 2011). The global sensitivity indices computed by Monte Carlo simulations reveal how the input (model parameters) variability influences the variability in the output (entrainment features).



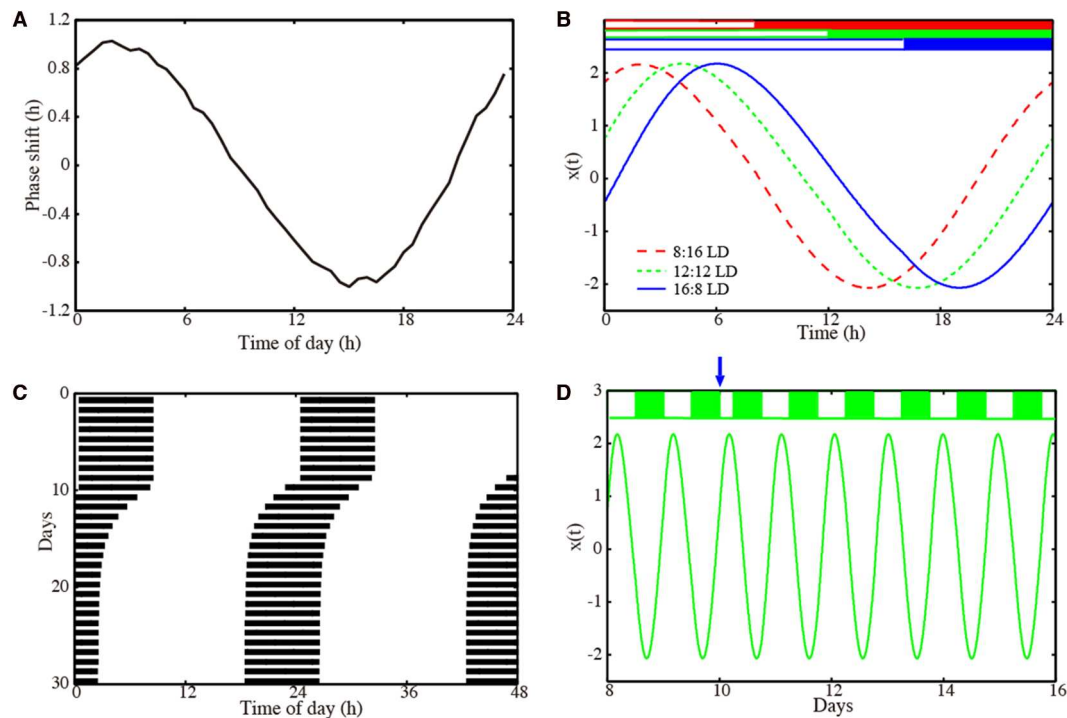


**FIGURE 2 |** Properties of our amplitude-phase model for a representative optimized parameter set. **(A)** Phase response curve with respect to a 6 h light pulse. **(B)** Waveforms  $x(t)$  of the oscillator entrained to *Zeitgeber* signals with 8:16 LD (dashed red line), 12:12 LD (dotted green line), and 16:8 LD (solid blue line). **(C)** Actogram of the oscillator, to which a 6 h advancing jet lag was induced on day 10. **(D)** Time-trace  $x(t)$  of the oscillators, to which a 6 h advancing jet lag was induced on day 10. Model parameters:  $\tau = 23.36$  h,  $A = 2.063$ ,  $\lambda = 0.386$  h<sup>-1</sup> with  $\omega = \frac{2\pi}{\tau}$ .

We have denoted an entrainment feature (i.e., re-entrainment time  $T_e$ , maximum shift  $\Delta\phi_{max}$ , or seasonal variability  $\Delta\psi$ ) as  $Y = \phi(X_1, X_2, X_3)$  using a scalar function  $\phi: \mathbb{R}^3 \rightarrow \mathbb{R}$ . The inputs  $\{X_1, X_2, X_3\}$  stand for random variables that represent the model parameters  $\{\tau, A, \lambda\}$ , respectively. The random variables are assumed to be uniformly distributed. The first-order sensitivity indices  $S_i$  for the input  $X_i$  ( $i = 1, 2, 3$ ) are defined as  $S_i = \text{Var}(E(Y|X_i))/\text{Var}(Y)$ , where  $\text{Var}$  and  $E$  are variance and expectation, respectively. The second-order sensitivity indices  $S_{ij}$  for the inputs  $X_i$  and  $X_j$  are defined as  $S_{ij} = \{\text{Var}(E(Y|X_i, X_j)) - \text{Var}(E(Y|X_i)) - \text{Var}(E(Y|X_j))\}/\text{Var}(Y)$ . The total sensitivity indices  $S_{T_i}$  for the input  $X_i$  are finally given by  $S_{T_i} = \sum_{k \# i} S_k$ , where  $\#i$  represents all the sets of indices that contain  $i$  (e.g.,  $S_{T_1} = S_1 + S_{12} + S_{13} + S_{123}$ ). These indices quantify the influence of the different inputs on the variance of  $Y$ . In our study, the Sobol indices were estimated with Monte-Carlo methods, where the number of randomly generated samples to estimate the indices was set to  $N = 10,000$ .

### 3. RESULTS AND DISCUSSIONS

#### 3.1. Models Reproduce PRC With Small Phase Shifts, Short Jet Lag, and Seasonality

We performed 200 successful parameter optimizations leading to an ensemble of parameter sets. We analyzed, in this section,

the parameters with a PRC having 1 h delay and advance. In **Figures S1, S2**, we also present parameter sets obtained with a modified optimization: in that case, we requested a PRC with a 2 h delay and advance. **Figure 2** shows results for a representative model obtained via optimization. The PRC in **Figure 2A** is almost sinusoidal with maximal delays and advances of 1 h as requested by the optimization. Simulations with different photoperiods are shown in **Figure 2B**. It is evident that there are major phase shifts due to the varying photoperiods. The small-amplitude PRC implies that phase shifts by light are limited. Consequently, long transients after jet lag might be expected. Interestingly, **Figure 2C** visualizes a relatively fast recovery from jet lag. **Figure 2D** illustrates the re-entrainment after a jet lag applied on day 10. Note that no pronounced amplitude changes were observed.

It turns out that simple models with just three free parameters can successfully reproduce phenotypic features. In particular, fast recovery from jet lag for PRCs with quite small phase shifts is surprising. We next exploited the ensembles of parameter sets to understand the underlying principles.

#### 3.2. Optimization Produced Highly Clustered Parameter Sets

In this section, we have focused on the 200 parameter sets with the  $\pm 1$  h PRCs exemplified in **Figure 2** (see **Figure S1** for  $\pm 2$  h PRCs).



The possible search ranges for our parameters were quite large (periods between 18 and 30 h, amplitudes between 0 and 5, and amplitude relaxation rates between 0 and  $0.5\text{h}^{-1}$ ). The histograms from the optimized parameter sets demonstrate that the search leads to quite specific values: periods of around  $23.3 \pm 0.1$  h, amplitudes of about  $2.1 \pm 0.04$ , and large relaxation rates of  $0.25 \pm 0.1\text{h}^{-1}$ .

The optimized amplitude can be easily understood from the constraint on PRCs: for a given pulse strength the PRC shrinks monotonically with increasing amplitude (Pittendrigh, 1981; Vitaterna et al., 2006). A large amplitude of about 2.1 can be understood as a result of PRC having small phase shifts ( $\pm 1$  h). In contrast, our optimizations with a  $\pm 2$  h PRC lead to smaller amplitudes around  $\pm 1.2$  (see **Figure S1b**).

Amplitude relaxation rates range between 0.07 and  $0.5\text{h}^{-1}$ . A value of  $0.07\text{h}^{-1}$  corresponds to a half-life of amplitude perturbations of about 10 h, while a value of  $0.5\text{h}^{-1}$  corresponds to a half-life of amplitude perturbations of about 1.4 h. Thus, all values in the histogram imply relatively fast amplitude relaxation. In Abraham et al. (2010), we termed limit cycles with fast amplitude relaxation “rigid oscillators.” Interestingly, Comas et al. (2007) found that two light pulses separated by 10 h shift phases almost independently. This finding confirms earlier studies of double pulses (Pittendrigh and Daan, 1976b). These observations are consistent with fast amplitude relaxation rates. Jet lag leads to a specific type of transient (compare **Figure 1B**). Thus, it seems reasonable that fast amplitude relaxation helps to achieve short transients after a jet lag.

The most surprising result of our optimization is the narrow range of intrinsic periods. We have argued that specific periods allow appropriate seasonal flexibility (compare **Figure 4**). In short, at specific parts of *Arnold* onions (i.e., the entrainment regions in the  $\kappa$ - $T$  parameter plane), the required 4 h phase

differences were found to give a reasonable phase shifts between 16:8 LD and 8:16 LD. We emphasize that specific periods (23.36 h in **Figure 2**, 24.64 h in **Figure S2**, 23.48 h in **Figure S6**) were not fitted to specific organisms.

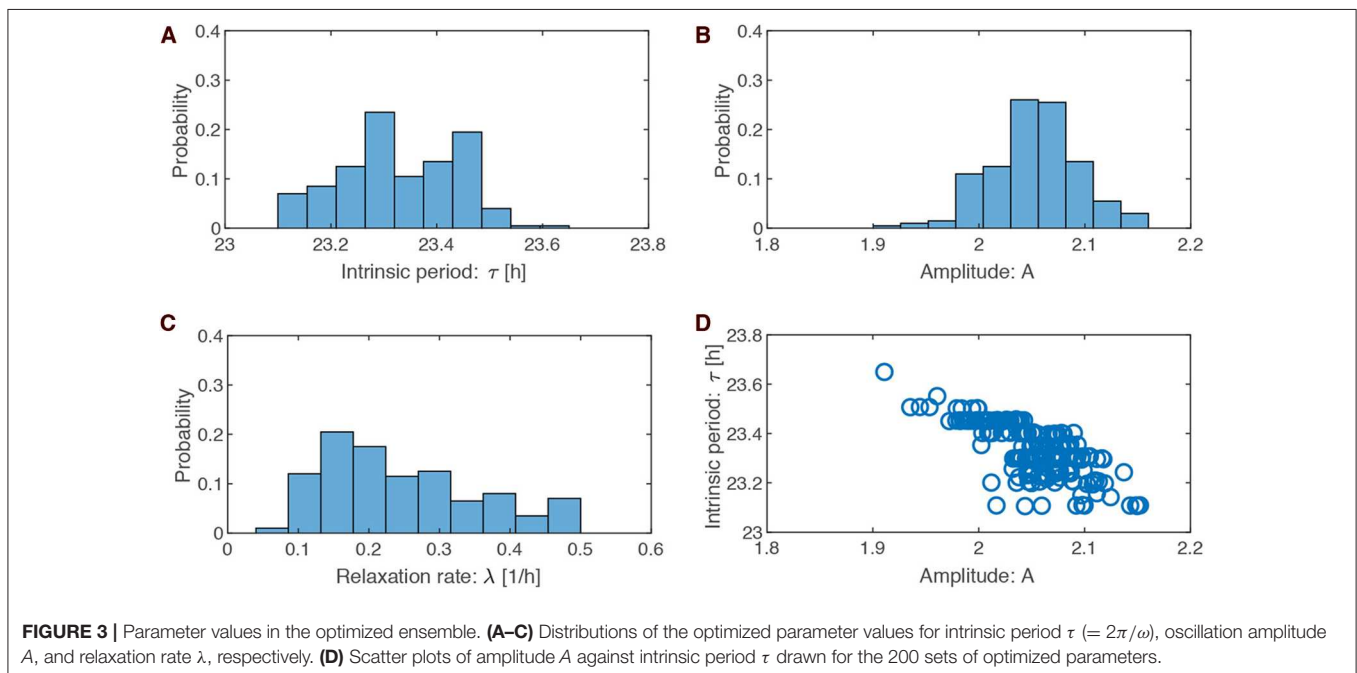
**Figure 3D** illustrates that the optimized parameter values are not independent. For instance, shorter periods are associated with larger amplitude. A possible explanation is that short periods imply larger effective pulse strength (a 6 h pulse is a larger part of a 23 h than a 24 h period) leading to larger amplitude in order to maintain the requested PRC amplitude.

In order to evaluate the robustness of our optimization approach, we generated also 200 parameter sets with PRCs with about a 2 h advance and delay. In these cases, we found intrinsic periods of  $24.6 \pm 0.1$  h, amplitudes of  $1.18 \pm 0.08$ , and relaxation rates of  $0.4 \pm 0.1\text{h}^{-1}$ . The relaxation rates and amplitude-period correlations were similar to the results with PRCs of about 1 h advance and delay (compare **Figure 3** and **Figure S1**).

It should be noted that the PRC and the intrinsic period are in a trade-off relationship (**Figures S3I, S4I, S5I**). For a quick recovery from advanced jet lag, a short period ( $< 24$  h) is advantageous, since the jet lag-induced phase shift is reduced everyday by the period difference to 24 h. A long period ( $> 24$  h), on the other hand, requires a stronger *Zeitgeber* forcing and thus PRC with larger phase shifts, since the phase shift is otherwise increased by the period difference to 24 h. For this reason,  $\pm 1$  h PRCs produced short periods, while  $\pm 2$  h PRCs led to longer periods.

### 3.3. Complex Association Between Model Parameter and Entrainment Features

Our global optimization provided 200 sets of parameters  $\{\tau, A, \lambda\}$  that reproduced the entrainment features of PRC with small phase shifts, fast recovery from jet lag, and high seasonal



variability. **Figures S3, S4** summarize the results for  $\pm 1$  h PRCs and  $\pm 2$  h PRCs, respectively. The upper 3 graphs show associations between the model parameters, illustrating that the parameters are not independent. The middle 9 graphs represent associations between the model parameters and the entrainment features (re-entrainment time  $T_e$ , maximum shift  $\Delta\varphi_{max}$ , seasonal variability  $\Delta\psi$ ), while the lower 3 graphs display associations between the entrainment features. The resulting patterns are quite complex and depend on specific constraints.

Since the recovery time from jet lag varies strongly even for mice from the same strain (Evans et al., 2015), we also optimized models for 3 day re-entrainment time instead of 2 day. The resulting scatter plots in **Figure S5** reveal interesting changes: the intrinsic periods range from 23.4 h to 24.3 h and there exists a parameter set with a rather low relaxation time of 75 h.

**TABLE 1** | Sobol's global sensitivity analysis, showing dependence of the entrainment features (re-entrainment time:  $T_e$ , maximum shift:  $\Delta\varphi_{max}$ , seasonal variability:  $\Delta\psi$ ) on the model parameters (intrinsic period:  $\tau$ , amplitude:  $A$ , relaxation rate:  $\lambda$ ).

	Parameters	Re-entrainment time ( $T_e$ )	Seasonality ( $\Delta\psi$ )	PRC size ( $\Delta\varphi_{max}$ )
Total	$\tau$	0.627	0.535	0.022
Sensitivity	$A$	0.724	0.777	0.823
$S_{T_i}$	$\lambda$	0.335	0.295	0.006
First-order	$\tau$	0.228	0.088	0.145
Sensitivity	$A$	0.174	0.233	0.967
$S_i$	$\lambda$	0.077	0.085	-0.012
Second-order	$\tau, A$	0.262	0.383	-0.118
Sensitivity	$\tau, \lambda$	-0.029	0.049	0.044
$S_{ij}$	$A, \lambda$	0.122	0.146	0.023

Thus, a relaxed jet lag constraint allows other periods and slow amplitude relaxation. Details regarding the parameter set with slow relaxation are provided in **Figure S6**. The recovery from jet lag is now accompanied by a small amplitude change as found in Goodwin models (Ananthasubramaniam et al., 2020) and the *Arnold* onion is less tilted as predicted (Schmal et al., 2015).

In order to quantify the complex associations of the model parameters and the entrainment features, we performed Sobol's global sensitivity analysis (Sobol, 1993, 2001; Morio, 2011). The strongest correlation was found between amplitude ( $A$ ) and PRC size ( $\Delta\varphi_{max}$ ), as expected (**Table 1**). Re-entrainment time ( $T_e$ ) and seasonal variability ( $\Delta\psi$ ) are influenced by all the model parameters ( $\tau$ ,  $A$ ,  $\lambda$ ). Second-order sensitivities reveal that the relaxation rate ( $\lambda$ ) effects re-entrainment time and seasonal variability in synergy with amplitude changes.

### 3.4. Arnold Onions Provide Insights Into the Optimized Parameters

To systematically investigate the impact of photoperiod ( $\kappa$ ) and Zeitgeber period ( $T$ ) on entrainment properties, we analyze in **Figure 4** two *Arnold* onions for representative parameter sets with a short period and a  $\pm 1$  h PRC as well as a large period and a  $\pm 2$  h PRC. Interestingly, the *Arnold* onions are tilted, i.e., the DD periods (constant darkness at photoperiod  $\kappa = 0$ ) are smaller than the LL periods (constant light at photoperiod  $\kappa = 1$ ) as predicted by *Aschoff's rule* for nocturnal animals (Aschoff, 1960). The largest entrainment range is found around a photoperiod of  $\kappa = 0.5$  as predicted by Wever (1964). As expected, a larger PRC implies a wider range of entrainment (compare sizes of the *Arnold* onion in **Figures 4A,B**).

The phase of entrainment is color-coded in **Figure 4**. It is evident that the phases vary strongly with the Zeitgeber period  $T$ . There are theoretical predictions that phases change by about 12 h (Wever, 1964; Granada et al., 2013; Bordyugov et al., 2015) for different *Zeitgeber* periods. Interestingly, the variation

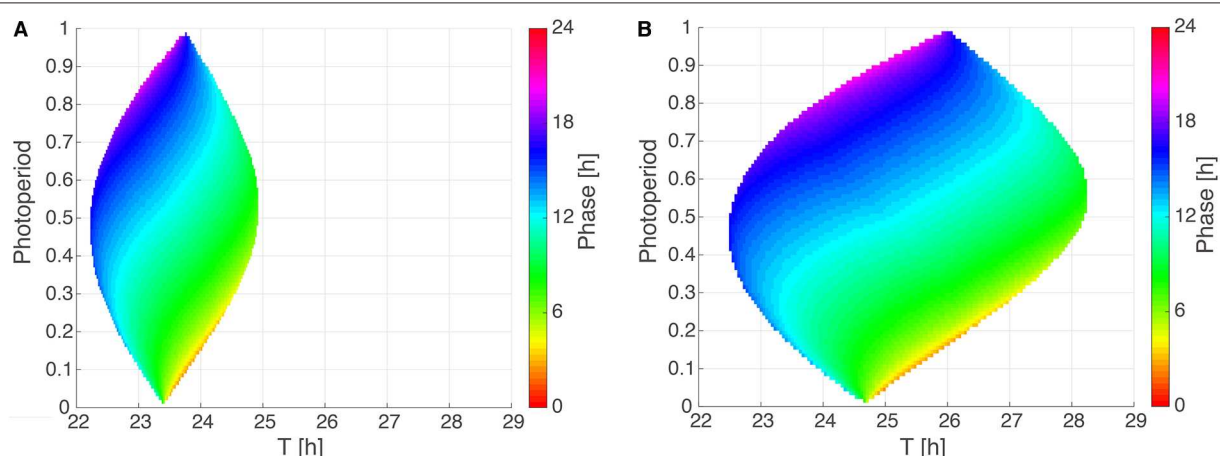


**FIGURE 4** | *Arnold* onions for the two PRC constraints. **(A,B)** 1:1 entrainment ranges in the  $\kappa$ - $T$  parameter plane (*Arnold* onions). Entrainment phases were determined by numerical simulations and have been color-coded within the region of entrainment. Panel **(A)** depicts an *Arnold* onion for an optimized parameter set with a  $\pm 1$  h PRC, a short-period  $\tau = 23.36$  h,  $A = 2.063$ , and  $\lambda = 0.386$  h<sup>-1</sup>. Panel **(B)** shows an *Arnold* onion for an optimized parameter set with a  $\pm 2$  h PRC, a long-period  $\tau = 24.64$  h,  $A = 1.144$ ,  $\lambda = 0.50$  h<sup>-1</sup>.

of photoperiods in the vertical direction implies also very pronounced variations of the entrainment phase. Consequently, we could find many parameter sets with about 4 h phase shift between photoperiods of  $\kappa = 1/3$  (8:16 LD) and of  $\kappa = 2/3$  (16:8 LD).

## 4. CONCLUSIONS AND OUTLOOK

### 4.1. Optimized Models Reproduce Phenotypic Features

In most cases, the circadian clock of vertebrates is characterized by a relatively small type 1 PRC, by a narrow entrainment range, by fast recovery from jet lag, and by pronounced seasonal flexibility. We addressed whether or not these phenotypic features can be reproduced by simple amplitude-phase models with just three free parameters: period, amplitude, and relaxation time. To our surprise, we found many parameter sets via global optimization that reproduced the phenotypic features.

The availability of many parameter sets derived from random optimization allows extraction of essential properties of successful models. It turned out that the amplitude  $A$  is adjusted to reproduce PRCs with small phase shifts for a given *Zeitgeber* strength  $Z$ . According to limit cycle theory (Pavlidis, 1969; Peterson, 1980), the strength of a perturbation is governed by the ratio  $Z/A$  of *Zeitgeber* strength to amplitude. This implies that large limit cycles exhibit small phase shifts for a fixed *Zeitgeber* strength (Vitaterna et al., 2006).

In all suitable models, we found relatively fast amplitude relaxation rates with half-lives of perturbations below 10 h. This “rigidity” of limit cycles (Abraham et al., 2010) can support fast relaxation to the new phase after jet lag (compare **Figure 1B**). Double pulse experiments (Pittendrigh and Daan, 1976b; Comas et al., 2007) are consistent with fast relaxation rates.

In order to reproduce seasonality, we optimized our model under the constraint that 16:8 and 8:16 LD cycles have entrainment phases that are about 4 h apart from each other. This implies that the phase could follow dusk or dawn (Daan and Aschoff, 1975). In other words, we requested that the entrainment phase depends strongly on the photoperiod. As illustrated in **Figure 4**, such a strong dependency is indeed reproduced by our simple amplitude-phase models. Our optimization procedure selected specific periods that lead to a 4 h phase variation between photoperiods  $\kappa = 1/3$  and  $\kappa = 2/3$ . Note that other periods can give large phase differences as well (compare the large vertical phase variations in **Figure 4**).

We have emphasized that our constraints were chosen to represent characteristic mammalian entrainment features: PRC with small phase shifts, relaxation from jet lag within a few days, and pronounced seasonal variability. Moreover, we based our constraints on light-pulse PRCs and considered only 6h-advanced jet lag. The observed increase of period with light intensity (compare **Figure 4**) resembles *Aschoff's rule* for nocturnal mammals.

Consequently, our results do not apply to clocks with type 0 PRCs and immediate phase resetting (Shaw and Brody, 2000; Devlin and Kay, 2001; Buhr et al., 2010). Furthermore, differences

between phase advances and delays were not addressed. Other studies (Locke et al., 2005; Lu et al., 2016; Ananthasubramaniam et al., 2020) show that oscillator theory can also help to understand differences between advances and delays.

### 4.2. Relevance of Phenomenological Amplitude-Phase Models

Simplistic models as studied in this paper are quite generally applicable (Ananthasubramaniam et al., 2020). In principle, they could be used to describe single cells, tissue clocks, and organismic data. For single cells, damped stochastic oscillators can represent the observations also surprisingly well (Westermarck et al., 2009). Such models have vanishingly small amplitudes and smaller relaxation rates, and they are driven by stochastic terms. Otherwise their complexity is comparable to our models discussed above.

The Poincaré model studied in this paper is particularly simple, since it has just three free parameters. Similar results on PRCs and entrainment have been described by other amplitude-phase models (Kronauer et al., 1982; Klerman et al., 1996; Flôres and Oda, 2020). The simplicity of our models implies that extensions are needed for fitting specific organisms and *Zeitgeber* profiles.

Complex models with multiple gene-regulatory feedback loops (Mirsky et al., 2009; Pokhilko et al., 2010; Relógio et al., 2011; Woller et al., 2016) could be reduced to amplitude-phase models simply by extracting periods, amplitudes, and relaxation rates from simulations. However, in such cases, the amplitudes are not uniquely defined since there are many dynamic variables.

### 4.3. How Can Circadian Amplitudes Be Defined?

This difficulty in defining amplitudes points to a general problem in chronobiology. Most studies focus on periods and entrainment phases. Limit cycle theory emphasizes that amplitudes are essential for understanding PRCs and entrainment. It is, however, not evident which amplitudes properly represent the limit cycle oscillator. Some studies consider gene expression levels (Lakin-Thomas et al., 1991; Wang et al., 2019) or reporter amplitudes (Leise et al., 2012), and other studies quantify activity rhythms (Bode et al., 2011; Erzberger et al., 2013). Since the ratio of *Zeitgeber* strength to amplitude  $Z/A$  governs PRCs and entrainment phases, we suggest that amplitudes could be quantified indirectly: the stronger the response to physiological perturbations, the smaller the amplitude. This approach leads to the concept of strong and weak oscillators (Abraham et al., 2010; Granada et al., 2013). Strong oscillators are robust and exhibit small phase shifts and narrow entrainment ranges but large phase variability (Granada et al., 2013). In this sense, wild-type vertebrate clocks represent strong oscillators in contrast to single cell organisms or plants. Indeed, the review of Aschoff and Pohl (1978) demonstrates impressively these properties.

Interestingly, a reduction in relative amplitudes (i.e., amplitudes as a fraction of the mesor) can reduce jet lag drastically, since resetting signals are much more efficient (An et al., 2013; Jagannath et al., 2013; Yamazaki et al., 2013).

#### 4.4. Arnold Onions Quantify Entrainment

As shown in **Figure 4**, *Arnold* onions represent entrainment ranges and phases of entrainment in a compact manner. Astonishingly, even quite basic models lead to really complex variations of entrainment phases. As expected, the period mismatch  $T-\tau$  has a rather strong effect on the entrainment phase. This reflects the well-known feature that short intrinsic periods  $\tau$  have earlier entrainment phases (“chronotypes”) (Pittendrigh and Daan, 1976b; Mellow et al., 1999; Duffy et al., 2001). These associations are reflected in the horizontal phase variations in the *Arnold* onion. Interestingly, the vertical phase variability is also quite large. This observation demonstrates that also the effective *Zeitgeber* strength  $Z/A$  and the photoperiod affect the phase of entrainment strongly. Consequently, the expected correlations between periods and entrainment phase could be masked by varying amplitudes, *Zeitgeber* strength, and photoperiods. In other words, chronotypes are governed by periods only if relative *Zeitgeber* strength and photoperiod are kept constant.

The complexity of entrainment phase regulation indicates that generic properties of coupled oscillators can provide useful insights in chronobiology. In particular, basic amplitude-phase models can help understand the control of jet lag and seasonality.

#### DATA AVAILABILITY STATEMENT

All datasets generated for this study are included in the article/**Supplementary Material**.

#### AUTHOR CONTRIBUTIONS

HH designed the study. IT performed the model simulations. IT, BA, CS, and HH discussed the results. HH wrote the main text. IT, BA, and CS revised the text.

#### ACKNOWLEDGMENTS

The authors thank Serge Daan (†), Achim Kramer, and Adrian Granada for stimulating discussions. IT acknowledges financial support from the Japan Society for the Promotion of Science (JSPS) (KAKENHI Nos. 16K00343, 17H06313, 18H02477, 19H01002, and 20K11875). BA, CS, and HH acknowledge support from the Deutsche Forschungsgemeinschaft (DFG) (SPP 2041, TRR 186-A16, and TRR 186-A17). In addition, CS acknowledges support from the DFG (SCH3362/2-1) and the JSPS (PE17780).

#### SUPPLEMENTARY MATERIAL

The Supplementary Material for this article can be found online at: <https://www.frontiersin.org/articles/10.3389/fphys.2020.00334/full#supplementary-material>

**Figure S1** | Results of parameter optimization based on cost function  $E(A, \omega, \lambda) = \frac{(T_e - 48h)^2}{(24h)^2} + \frac{(\Delta\varphi_{max} - 2h)^2}{(1h)^2} + \frac{(\Delta\psi - 4h)^2}{(4h)^2}$ , where  $\pm 2$  h PRC was requested. **(a–c)** Distributions of the 200 optimized parameter sets for  $\tau$  ( $24.6 \pm 0.1$  h),  $A$  ( $1.18 \pm 0.08$ ),  $\lambda$  ( $0.4 \pm 0.1$  h<sup>-1</sup>), respectively. **(d)** Scatter plots of amplitude  $A$  against intrinsic period  $\tau$  drawn for 200 sets of optimized parameters.

**Figure S2** | Simulation of the amplitude-phase oscillator model using one of the 200 parameter sets optimized for a  $\pm 2$  h PRC. **(a)** Phase response curve with respect to a 6 h light pulse. **(b)** Waveforms  $x(t)$  of the oscillator entrained to *Zeitgeber* signals with 8:16 LD (dashed red line), 12:12 LD (dotted green line), and 16:8 LD (solid blue line). **(c)** Actogram drawn for the oscillator, to which a 6 h advancing jet lag was induced on day 10. **(d)** Time-trace  $x(t)$  of the oscillators, to which a 6 h advancing jet lag was induced on the 10th day. Parameter values:  $\tau = 24.64$  h,  $A = 1.144$ ,  $\lambda = 0.50$  h<sup>-1</sup>.

**Figure S3** | Scatter plots for 200 data sets optimized for  $\pm 1$  h PRC with cost function  $E(A, \omega, \lambda) = \frac{(T_e - 48h)^2}{(24h)^2} + \frac{(\Delta\varphi_{max} - 1h)^2}{(1h)^2} + \frac{(\Delta\psi - 4h)^2}{(4h)^2}$ . **(a)** Amplitude  $A$  vs. relaxation rate  $\lambda$ . **(b)** Amplitude  $A$  vs. intrinsic period  $\tau$ . **(c)** Relaxation rate  $\lambda$  vs. intrinsic period  $\tau$ . **(d)** Amplitude  $A$  vs. re-entrainment time  $T_e$ . **(e)** Amplitude  $A$  vs. phase variability  $\Delta\psi$ . **(f)** Amplitude  $A$  vs. maximum PRC  $\Delta\varphi_{max}$ . **(g)** Relaxation rate  $\lambda$  vs. re-entrainment time  $T_e$ . **(h)** Relaxation rate  $\lambda$  vs. phase variability  $\Delta\psi$ . **(i)** Relaxation rate  $\lambda$  vs. maximum PRC  $\Delta\varphi_{max}$ . **(j)** Intrinsic period  $\tau$  vs. re-entrainment time  $T_e$ . **(k)** Intrinsic period  $\tau$  vs. phase variability  $\Delta\psi$ . **(l)** Intrinsic period  $\tau$  vs. maximum PRC  $\Delta\varphi_{max}$ . **(m)** Re-entrainment time  $T_e$  vs. phase variability  $\Delta\psi$ . **(n)** Re-entrainment time  $T_e$  vs. maximum PRC  $\Delta\varphi_{max}$ . **(o)** Phase variability  $\Delta\psi$  vs. maximum PRC  $\Delta\varphi_{max}$ .

**Figure S4** | Scatter plots for 200 data sets optimized for  $\pm 2$  h PRC with cost function  $E(A, \omega, \lambda) = \frac{(T_e - 48h)^2}{(24h)^2} + \frac{(\Delta\varphi_{max} - 2h)^2}{(1h)^2} + \frac{(\Delta\psi - 4h)^2}{(4h)^2}$ . **(a)** Amplitude  $A$  vs. relaxation rate  $\lambda$ . **(b)** Amplitude  $A$  vs. intrinsic period  $\tau$ . **(c)** Relaxation rate  $\lambda$  vs. intrinsic period  $\tau$ . **(d)** Amplitude  $A$  vs. re-entrainment time  $T_e$ . **(e)** Amplitude  $A$  vs. phase variability  $\Delta\psi$ . **(f)** Amplitude  $A$  vs. maximum PRC  $\Delta\varphi_{max}$ . **(g)** Relaxation rate  $\lambda$  vs. re-entrainment time  $T_e$ . **(h)** Relaxation rate  $\lambda$  vs. phase variability  $\Delta\psi$ . **(i)** Relaxation rate  $\lambda$  vs. maximum PRC  $\Delta\varphi_{max}$ . **(j)** Intrinsic period  $\tau$  vs. re-entrainment time  $T_e$ . **(k)** Intrinsic period  $\tau$  vs. phase variability  $\Delta\psi$ . **(l)** Intrinsic period  $\tau$  vs. maximum PRC  $\Delta\varphi_{max}$ . **(m)** Re-entrainment time  $T_e$  vs. phase variability  $\Delta\psi$ . **(n)** Re-entrainment time  $T_e$  vs. maximum PRC  $\Delta\varphi_{max}$ . **(o)** Phase variability  $\Delta\psi$  vs. maximum PRC  $\Delta\varphi_{max}$ .

**Figure S5** | Scatter plots for 200 data sets optimized for  $\pm 1$  h PRC and 3 days re-entrainment time with cost function  $E(A, \omega, \lambda) = \frac{(T_e - 72h)^2}{(24h)^2} + \frac{(\Delta\varphi_{max} - 1h)^2}{(1h)^2} + \frac{(\Delta\psi - 4h)^2}{(4h)^2}$ . **(a)** Amplitude  $A$  vs. relaxation rate  $\lambda$ . **(b)** Amplitude  $A$  vs. intrinsic period  $\tau$ . **(c)** Relaxation rate  $\lambda$  vs. intrinsic period  $\tau$ . **(d)** Amplitude  $A$  vs. re-entrainment time  $T_e$ . **(e)** Amplitude  $A$  vs. phase variability  $\Delta\psi$ . **(f)** Amplitude  $A$  vs. maximum PRC  $\Delta\varphi_{max}$ . **(g)** Relaxation rate  $\lambda$  vs. re-entrainment time  $T_e$ . **(h)** Relaxation rate  $\lambda$  vs. phase variability  $\Delta\psi$ . **(i)** Relaxation rate  $\lambda$  vs. maximum PRC  $\Delta\varphi_{max}$ . **(j)** Intrinsic period  $\tau$  vs. re-entrainment time  $T_e$ . **(k)** Intrinsic period  $\tau$  vs. phase variability  $\Delta\psi$ . **(l)** Intrinsic period  $\tau$  vs. maximum PRC  $\Delta\varphi_{max}$ . **(m)** Re-entrainment time  $T_e$  vs. phase variability  $\Delta\psi$ . **(n)** Re-entrainment time  $T_e$  vs. maximum PRC  $\Delta\varphi_{max}$ . **(o)** Phase variability  $\Delta\psi$  vs. maximum PRC  $\Delta\varphi_{max}$ .

**Figure S6** | Entrainment features of the amplitude-phase model for  $\tau = 23.48$  h,  $A = 2.458$ ,  $\lambda = 0.0134$  h<sup>-1</sup> with  $\omega = 0.268$ . **(a)** The re-entrainment process of the oscillator after its phase is shifted by a 6 h-advanced jet lag. The red line represents the trajectory that the system converges to. **(b)** Phase response curve with respect to a 6 h light pulse. **(c)** Waveforms  $x(t)$  of the oscillator entrained to *Zeitgeber* signal with 8:16 LD (purple), 12:12 LD (green), and 16:8 LD (blue). **(d)** Actogram drawn for the oscillator, to which a 6 h-advanced jet lag was induced on day 10. **(e)** Time-trace  $x(t)$  of the oscillators, to which a 6 h-advanced jet lag was induced on day 10. **(f)** *Arnold* onion (1:1 entrainment ranges in the  $x$ - $T$  parameter plane).



## REFERENCES

- Abraham, U., Granada, A. E., Westermark, P. O., Heine, M., Kramer, A., and Herzl, H. (2010). Coupling governs entrainment range of circadian clocks. *Mol. Syst. Biol.* 6:438. doi: 10.1038/msb.2010.92
- An, S., Harang, R., Meeker, K., Granados-Fuentes, D., Tsai, C. A., Mazuski, C., et al. (2013). A neuropeptide speeds circadian entrainment by reducing intercellular synchrony. *Proc. Natl. Acad. Sci. U.S.A.* 110, E4355–E4361. doi: 10.1073/pnas.1307088110
- Ananthasubramanian, B., Schmal, C., and Herzl, H. (2020). Amplitude effects allow short jetlags and large seasonal phase shifts in minimal clock models. *J. Mol. Biol.* doi: 10.1016/j.jmb.2020.01.014
- Aschoff, J. (1960). “Exogenous and endogenous components in circadian rhythms,” in *Cold Spring Harbor Symposia on Quantitative Biology*, ed L. Frisch, Vol. 25 (New York, NY: Cold Spring Harbor Laboratory Press), 11–28. doi: 10.1101/SQB.1960.025.01.004
- Aschoff, J., and Pohl, H. (1978). Phase relations between a circadian rhythm and its Zeitgeber within the range of entrainment. *Naturwissenschaften* 65, 80–84. doi: 10.1007/BF00440545
- Becker-Weimann, S., Wolf, J., Herzl, H., and Kramer, A. (2004). Modeling feedback loops of the mammalian circadian oscillator. *Biophys. J.* 87, 3023–3034. doi: 10.1529/biophysj.104.040824
- Bellman, J., Kim, J. K., Lim, S., and Hong, C. I. (2018). Modeling reveals a key mechanism for light-dependent phase shifts of neurospora circadian rhythms. *Biophys. J.* 115, 1093–1102. doi: 10.1016/j.bpj.2018.07.029
- Bode, B., Shahmoradi, A., Rossner, M. J., and Oster, H. (2011). Genetic interaction of *per1* and *dec1/2* in the regulation of circadian locomotor activity. *J. Biol. Rhythms* 26, 530–540. doi: 10.1177/0748730411419782
- Bordyugov, G., Abraham, U., Granada, A., Rose, P., Imkeller, K., Kramer, A., et al. (2015). Tuning the phase of circadian entrainment. *J. R. Soc. Interface* 12:108. doi: 10.1098/rsif.2015.0282
- Buhr, E. D., Yoo, S.-H., and Takahashi, J. S. (2010). Temperature as a universal resetting cue for mammalian circadian oscillators. *Science* 330, 379–385. doi: 10.1126/science.1195262
- Comas, M., Beersma, D., Spoelstra, K., and Daan, S. (2006). Phase and period responses of the circadian system of mice (*Mus musculus*) to light stimuli of different duration. *J. Biol. Rhythms* 21, 362–372. doi: 10.1177/0748730406292446
- Comas, M., Beersma, D., Spoelstra, K., and Daan, S. (2007). Circadian response reduction in light and response restoration in darkness: a “skeleton” light pulse PRC study in mice (*Mus musculus*). *J. Biol. Rhythms* 22, 432–444. doi: 10.1177/0748730407305728
- Czeisler, C. A., Duffy, J. F., Shanahan, T. L., Brown, E. N., Mitchell, J. F., Rimmer, D. W., et al. (1999). Stability, precision, and near-24-h period of the human circadian pacemaker. *Science* 284, 2177–2181. doi: 10.1126/science.284.5423.2177
- Daan, S., and Aschoff, J. (1975). Circadian rhythms of locomotor activity in captive birds and mammals: their variations with season and latitude. *Oecologia* 18, 269–316. doi: 10.1007/BF00345851
- Daan, S., and Berde, C. (1978). Two coupled oscillators: simulations of the circadian pacemaker in mammalian activity rhythms. *J. Theor. Biol.* 70, 297–313. doi: 10.1016/0022-5193(78)90378-8
- Devlin, P. F., and Kay, S. A. (2001). Circadian photoperception. *Annu. Rev. Physiol.* 63, 677–694. doi: 10.1146/annurev.physiol.63.1.677
- Dibner, C., Schibler, U., and Albrecht, U. (2010). The mammalian circadian timing system: organization and coordination of central and peripheral clocks. *Annu. Rev. Physiol.* 72, 517–549. doi: 10.1146/annurev-physiol-021909-135821
- Dodd, A. N., Salathia, N., Hall, A., Kévei, E., Tóth, R., Nagy, F., et al. (2005). Plant circadian clocks increase photosynthesis, growth, survival, and competitive advantage. *Science* 309, 630–633. doi: 10.1126/science.1115581
- Duffing, G. (1918). *Erzwungene Schwingungen bei veränderlicher Eigenfrequenz und ihre technische Bedeutung*. Braunschweig: F. Vieweg & Sohn.
- Duffy, J. F., Rimmer, D. W., and Czeisler, C. A. (2001). Association of intrinsic circadian period with morningness-eveningness, usual wake time, and circadian phase. *Behav. Neurosci.* 115, 895–899. doi: 10.1037/0735-7044.115.4.895
- Eberhart, R., and Kennedy, J. (1995). “Particle swarm optimization,” in *Proceedings of the IEEE International Conference on Neural Networks*, Vol. 4 (Perth, WA: Citeseer), 1942–1948.
- Erzberger, A., Hampf, G., Granada, A., Albrecht, U., and Herzl, H. (2013). Genetic redundancy strengthens the circadian clock leading to a narrow entrainment range. *J. R. Soc. Interface* 10:20130221. doi: 10.1098/rsif.2013.0221
- Evans, J. A., Leise, T. L., Castanon-Cervantes, O., and Davidson, A. J. (2015). Neural correlates of individual differences in circadian behaviour. *Proc. R. Soc. B Biol. Sci.* 282:20150769. doi: 10.1098/rspb.2015.0769
- Flóres, D. E., and Oda, G. A. (2020). Quantitative study of dual circadian oscillator models under different skeleton photoperiods. *J. Biol. Rhythms*. doi: 10.1177/0748730420901939
- Forger, D. B., and Peskin, C. S. (2003). A detailed predictive model of the mammalian circadian clock. *Proc. Natl. Acad. Sci. U.S.A.* 100, 14806–14811. doi: 10.1073/pnas.2036281100
- Glass, L., and Mackey, M. C. (1988). *From Clocks to Chaos: The Rhythms of Life*. Princeton, NJ: Princeton University Press.
- Granada, A. E., Bordyugov, G., Kramer, A., and Herzl, H. (2013). Human chronotypes from a theoretical perspective. *PLoS ONE* 8:e59464. doi: 10.1371/journal.pone.0059464
- Granada, A. E., Hennig, R. M., Ronacher, B., Kramer, A., and Herzl, H. (2009). Phase response curves: elucidating the dynamics of coupled oscillators. *Methods Enzymol.* 454, 1–27. doi: 10.1016/S0076-6879(08)03801-9
- Hardin, P. E., Hall, J. C., and Rosbash, M. (1990). Feedback of the *Drosophila* period gene product on circadian cycling of its messenger RNA levels. *Nature* 343, 536–540. doi: 10.1038/343536a0
- Hastings, M. H., Maywood, E. S., and Brancaccio, M. (2018). Generation of circadian rhythms in the suprachiasmatic nucleus. *Nat. Rev. Neurosci.* 19, 453–469. doi: 10.1038/s41583-018-0026-z
- Hazlerigg, D. G., and Wagner, G. C. (2006). Seasonal photoperiodism in vertebrates: from coincidence to amplitude. *Trends Endocrinol. Metab.* 17, 83–91. doi: 10.1016/j.tem.2006.02.004
- Honma, K.-i., Hashimoto, S., Nakao, M., and Honma, S. (2003). Period and phase adjustments of human circadian rhythms in the real world. *J. Biol. Rhythms* 18, 261–270. doi: 10.1177/0748730403018003008
- Huygens, C. (1986). *Horologium Oscillatorium (“The Pendulum Clock, or Geometrical Demonstrations Concerning the Motion of Pendula as Applied to Clocks” Translated by Richard J. Blackwell)*. Ames, IA: Iowa State University Press.
- Jagannath, A., Butler, R., Godinho, S. I., Couch, Y., Brown, L. A., Vasudevan, S. R., et al. (2013). The CRTCl-SIK1 pathway regulates entrainment of the circadian clock. *Cell* 154, 1100–1111. doi: 10.1016/j.cell.2013.08.004
- Johnson, C. H. (1992). “Phase response curves: what can they tell us about circadian clocks,” in *Circadian Clocks From Cell to Human*, eds T. Hiroshige and K.-I. Honma (Sapporo: Hokkaido University Press), 209–249.
- Khalsa, S. B. S., Jewett, M. E., Cajochen, C., and Czeisler, C. A. (2003). A phase response curve to single bright light pulses in human subjects. *J. Physiol.* 549, 945–952. doi: 10.1113/jphysiol.2003.040477
- Klerman, E. B., Dijk, D., Kronauer, R. E., and Czeisler, C. A. (1996). Simulations of light effects on the human circadian pacemaker: implications for assessment of intrinsic period. *Am. J. Physiol. Regul. Integr. Comp. Physiol.* 270, R271–R282. doi: 10.1152/ajpregu.1996.270.1.R271
- Klotter, K. (1960). “Theoretical analysis of some biological models,” in *Cold Spring Harbor Symposia on Quantitative Biology*, ed L. Frisch, Vol. 25 (New York, NY: Cold Spring Harbor Laboratory Press), 189–196. doi: 10.1101/SQB.1960.025.01.017
- Kori, H., Yamaguchi, Y., and Okamura, H. (2017). Accelerating recovery from jet lag: prediction from a multi-oscillator model and its experimental confirmation in model animals. *Sci. Rep.* 7:46702. doi: 10.1038/srep46702
- Kronauer, R. E., Czeisler, C. A., Pilato, S. F., Moore-Ede, M. C., and Weitzman, E. D. (1982). Mathematical model of the human circadian system with two interacting oscillators. *Am. J. Physiol. Regul. Integr. Comp. Physiol.* 242, R3–R17. doi: 10.1152/ajpregu.1982.242.1.R3
- Kuramoto, Y. (1984). *Chemical Oscillations, Waves, and Turbulence*. Berlin: Springer.
- Lakin-Thomas, P. L., Brody, S., and Coté, G. G. (1991). Amplitude model for the effects of mutations and temperature on period and phase

- resetting of the neurospora circadian oscillator. *J. Biol. Rhythms* 6, 281–297. doi: 10.1177/074873049100600401
- Leise, T. L., Wang, C. W., Gitis, P. J., and Welsh, D. K. (2012). Persistent cell-autonomous circadian oscillations in fibroblasts revealed by six-week single-cell imaging of per2:: Luc bioluminescence. *PLoS ONE* 7:e33334. doi: 10.1371/journal.pone.0033334
- Leloup, J.-C., and Goldbeter, A. (2003). Toward a detailed computational model for the mammalian circadian clock. *Proc. Natl. Acad. Sci. U.S.A.* 100, 7051–7056. doi: 10.1073/pnas.1132112100
- Locke, J. C., Millar, A. J., and Turner, M. S. (2005). Modelling genetic networks with noisy and varied experimental data: the circadian clock in *Arabidopsis thaliana*. *J. Theor. Biol.* 234, 383–393. doi: 10.1016/j.jtbi.2004.11.038
- Locke, J. C., Westermark, P. O., Kramer, A., and Herzel, H. (2008). Global parameter search reveals design principles of the mammalian circadian clock. *BMC Syst. Biol.* 2:22. doi: 10.1186/1752-0509-2-22
- Loros, J. J., and Dunlap, J. C. (2001). Genetic and molecular analysis of circadian rhythms in neurospora. *Annu. Rev. Physiol.* 63, 757–794. doi: 10.1146/annurev.physiol.63.1.757
- Lu, Z., Klein-Cardena, K., Lee, S., Antonsen, T. M., Girvan, M., and Ott, E. (2016). Resynchronization of circadian oscillators and the east-west asymmetry of jet-lag. *Chaos* 26:094811. doi: 10.1063/1.4954275
- Merrow, M., Brunner, M., and Roenneberg, T. (1999). Assignment of circadian function for the neurospora clock gene frequency. *Nature* 399, 584–586. doi: 10.1038/21190
- Mirsky, H. P., Liu, A. C., Welsh, D. K., Kay, S. A., and Doyle, F. J. (2009). A model of the cell-autonomous mammalian circadian clock. *Proc. Natl. Acad. Sci. U.S.A.* 106, 11107–11112. doi: 10.1073/pnas.0904837106
- Morio, J. (2011). Global and local sensitivity analysis methods for a physical system. *Eur. J. Phys.* 32:1577. doi: 10.1088/0143-0807/32/6/011
- Ouyang, Y., Andersson, C. R., Kondo, T., Golden, S. S., and Johnson, C. H. (1998). Resonating circadian clocks enhance fitness in cyanobacteria. *Proc. Natl. Acad. Sci. U.S.A.* 95, 8660–8664. doi: 10.1073/pnas.95.15.8660
- Pavlidis, T. (1969). Populations of interacting oscillators and circadian rhythms. *J. Theor. Biol.* 22, 418–436. doi: 10.1016/0022-5193(69)90014-9
- Pavlidis, T. (1973). The free-run period of circadian rhythms and phase response curves. *Am. Natural.* 107, 524–530. doi: 10.1086/282855
- Peterson, E. L. (1980). A limit cycle interpretation of a mosquito circadian oscillator. *J. Theor. Biol.* 84, 281–310. doi: 10.1016/S0022-5193(80)80008-7
- Pikovsky, A., Rosenblum, M., and Kurths, J. (2003). *Synchronization: A Universal Concept in Nonlinear Sciences*, Vol. 12. Cambridge: Cambridge University Press.
- Pittendrigh, C. S. (1981). “Circadian systems: entrainment,” in *Biological Rhythms* ed J. Aschoff (Boston, MA: Springer), 95–124. doi: 10.1007/978-1-4615-6552-9\_7
- Pittendrigh, C. S., and Daan, S. (1976a). A functional analysis of circadian pacemakers in nocturnal rodents I. The stability and lability of spontaneous frequency. *J. Comp. Physiol.* 106, 223–252. doi: 10.1007/BF01417856
- Pittendrigh, C. S., and Daan, S. (1976b). A functional analysis of circadian pacemakers in nocturnal rodents IV. Entrainment: pacemaker as clock. *J. Comp. Physiol.* 106, 291–331. doi: 10.1007/BF01417859
- Pokhilko, A., Hodge, S. K., Stratford, K., Knox, K., Edwards, K. D., Thomson, A. W., et al. (2010). Data assimilation constrains new connections and components in a complex, eukaryotic circadian clock model. *Mol. Syst. Biol.* 6:416. doi: 10.1038/msb.2010.69
- Reddy, A., Field, M., Maywood, E., and Hastings, M. (2002). Differential resynchronization of circadian clock gene expression within the suprachiasmatic nuclei of mice subjected to experimental jet lag. *J. Neurosci.* 22, 7326–7330. doi: 10.1523/JNEUROSCI.22-17-07326.2002
- Relógio, A., Westermark, P. O., Wallach, T., Schellenberg, K., Kramer, A., and Herzel, H. (2011). Tuning the mammalian circadian clock: robust synergy of two loops. *PLoS Comput. Biol.* 7:e1002309. doi: 10.1371/journal.pcbi.1002309
- Rémi, J., Merrow, M., and Roenneberg, T. (2010). A circadian surface of entrainment: varying T,  $\tau$ , and photoperiod in *Neurospora crassa*. *J. Biol. Rhythms* 25, 318–328. doi: 10.1177/0748730410379081
- Schmal, C., Myung, J., Herzel, H., and Bordyugov, G. (2015). A theoretical study on seasonality. *Front. Neurol.* 6:94. doi: 10.3389/fneur.2015.00094
- Shaw, J., and Brody, S. (2000). Circadian rhythms in neurospora: a new measurement, the reset zone. *J. Biol. Rhythms* 15, 225–240. doi: 10.1177/074873040001500304
- Sobol, I. M. (1993). Sensitivity estimates for nonlinear mathematical models. *Math. Modell. Comput. Exp.* 1, 407–414.
- Sobol, I. M. (2001). Global sensitivity indices for nonlinear mathematical models and their monte carlo estimates. *Math. Comput. Simul.* 55, 271–280. doi: 10.1016/S0378-4754(00)00270-6
- Strogatz, S. (2004). *Sync: The Emerging Science of Spontaneous Order*. London: Penguin.
- Trelea, I. C. (2003). The particle swarm optimization algorithm: convergence analysis and parameter selection. *Inform. Process. Lett.* 85, 317–325. doi: 10.1016/S0020-0190(02)00447-7
- Van der Pol, B., and Van der Mark, J. (1927). Frequency demultiplication. *Nature* 120, 363–364. doi: 10.1038/120363a0
- Vansteensel, M. J., Yamazaki, S., Albus, H., Deboer, T., Block, G. D., and Meijer, J. H. (2003). Dissociation between circadian per1 and neuronal and behavioral rhythms following a shifted environmental cycle. *Curr. Biol.* 13, 1538–1542. doi: 10.1016/S0960-9822(03)00560-8
- Vitaterna, M. H., Ko, C. H., Chang, A.-M., Buhr, E. D., Fruechte, E. M., Schook, A., et al. (2006). The mouse clock mutation reduces circadian pacemaker amplitude and enhances efficacy of resetting stimuli and phase-response curve amplitude. *Proc. Natl. Acad. Sci. U.S.A.* 103, 9327–9332. doi: 10.1073/pnas.0603601103
- Wang, B., Kettenbach, A. N., Zhou, X., Loros, J. J., and Dunlap, J. C. (2019). The phospho-code determining circadian feedback loop closure and output in neurospora. *Mol. Cell* 74, 771–784. doi: 10.1016/j.molcel.2019.03.003
- Westermark, P. O., Welsh, D. K., Okamura, H., and Herzel, H. (2009). Quantification of circadian rhythms in single cells. *PLoS Comput. Biol.* 5:e1000580. doi: 10.1371/journal.pcbi.1000580
- Wever, R. (1962). Zum mechanismus der biologischen 24-stunden-periodik. *Kybernetik* 1, 139–154. doi: 10.1007/BF00289033
- Wever, R. (1964). Zum mechanismus der biologischen 24-stunden-periodik: III. Mitteilung anwendung der modell-gleichung. *Kybernetik* 2, 127–144. doi: 10.1007/BF00306797
- Wever, R. A. (1979). *The Circadian System of Man: Results of Experiments Under Temporal Isolation*. New York, NY: Springer-Verlag.
- Winfree, A. T. (1980). *The Geometry of Biological Time*. New York, NY; Heidelberg; Berlin: Springer-Verlag. doi: 10.1007/978-3-662-22492-2
- Woller, A., Duez, H., Staels, B., and Lefranc, M. (2016). A mathematical model of the liver circadian clock linking feeding and fasting cycles to clock function. *Cell Rep.* 17, 1087–1097. doi: 10.1016/j.celrep.2016.09.060
- Wyse, C., Coogan, A., Selman, C., Hazlerigg, D., and Speakman, J. (2010). Association between mammalian lifespan and circadian free-running period: the circadian resonance hypothesis revisited. *Biol. Lett.* 6, 696–698. doi: 10.1098/rsbl.2010.0152
- Yamaguchi, Y., Suzuki, T., Mizoro, Y., Kori, H., Okada, K., Chen, Y., et al. (2013). Mice genetically deficient in vasopressin v1a and v1b receptors are resistant to jet lag. *Science* 342, 85–90. doi: 10.1126/science.1238599
- Yamazaki, S., Numano, R., Abe, M., Hida, A., Takahashi, R.-I., Ueda, M., et al. (2000). Resetting central and peripheral circadian oscillators in transgenic rats. *Science* 288, 682–685. doi: 10.1126/science.288.5466.682
- Zhou, M., Kim, J. K., Eng, G.W. L., Forger, D. B., and Virshup, D. M. (2015). A period2 phosphoswitch regulates and temperature compensates circadian period. *Mol. Cell* 60, 77–88. doi: 10.1016/j.molcel.2015.08.022

**Conflict of Interest:** The authors declare that the research was conducted in the absence of any commercial or financial relationships that could be construed as a potential conflict of interest.

Copyright © 2020 Tokuda, Schmal, Ananthasubramaniam and Herzel. This is an open-access article distributed under the terms of the Creative Commons Attribution License (CC BY). The use, distribution or reproduction in other forums is permitted, provided the original author(s) and the copyright owner(s) are credited and that the original publication in this journal is cited, in accordance with accepted academic practice. No use, distribution or reproduction is permitted which does not comply with these terms.